Impacts of Connected Automated Vehicles on Freeway Traffic Patterns at Different Penetration Levels

Sergei S. Avedisov, *Member, IEEE*, Gaurav Bansal, and Gábor Orosz, *Member, IEEE*

***Abstract*— In this paper we investigate the effects of connected automated vehicles on traffic patterns. We first experimentally study traffic patterns using two connected human-driven vehicles, which are equipped with vehicle-to-vehicle (V2V) communication, and a connected automated vehicle, which is able to respond to V2V information and control its longitudinal motion. Our experimental results indicate the long-range feedback may benefit traffic flow and that car-following models with delay are able to replicate the experimental results. The data fitted models are used in simulations for a 100-car network to study traffic dynamics with partial penetration of connected automated vehicles.**

***Index Terms*— Connected automated vehicles, V2X communication, traffic flow.**

I. Introduction

RECENT developments in vehicle automation and advanced driver assistance systems (ADAS) led to significant improvements in vehicle safety. However, mobility of roadways has not witnessed a similar trend. The limiting effect of vehicle automation on mobility can be attributed to the limited sensory range, as traffic patterns such as congestion waves or stop-and-go traffic jams occur on a much larger scale than the ranges of cameras, lidars, and radars [1], [2]. Obstructions such as blind turns or other vehicles may further limit the range of these sensors.

The range limitations of sensors can be bypassed by using wireless vehicle-to-everything (V2X) communication [3]–[6]. Vehicles equipped with V2X communication, called connected vehicles, can send and receive messages over hundreds of meters and through obstructions such as blind corners or large vehicles. An automated vehicle equipped with V2X communications, called connected automated vehicle, can then respond to large-scale traffic patterns to mitigate congestion [7], [8]. The arising connected vehicle network is composed of regular human-driven vehicles, connected human-driven vehicles, and connected automated vehicles may potentially have a higher throughput than a traffic network composed of human-driven vehicles only.

The various merits of connected automated vehicles in connected vehicle networks have been investigated using analytical techniques and numerical simulations [9]–[13]. The strategies to control connected automated vehicles depend on the goals as well as the specific layout of the connected vehicle network. A popular strategy is called cooperative adaptive cruise control (CACC) [14]–[20] where several connected automated vehicles form a platoon. Another strategy called connected cruise control (CCC) where each connected automated vehicle utilizes information from surrounding connected human-driven vehicles to control their motion [21]–[24]. Experimental work for CACC, CCC, and other strategies has been performed with small fleets of vehicles to demonstrate safety and fuel economy improvements [16], [25]. The effects of such strategies on large-scale traffic patterns however has not been extensively studied due to the fact that such patterns need to traverse a large number of vehicles to develop. In this paper we focus on some characteristic traffic patterns (homogeneous flow, traveling waves, stop-and-go traffic) that can be reproduced by single-lane experiments. Studying more complex traffic patters, such as those shown in [26], are left for future research.

To evaluate the effects of long-range feedback on traffic patterns, we present an experimental setup for a connected vehicle network consisting of two human-driven connected vehicles and a connected automated vehicle. Our setup uses a periodic boundary condition, that is frequently used to study traffic patterns both analytically and experimentally [27]–[32]. However, instead of using a physical ring road to enforce the periodic boundary condition; we implement the periodic boundary condition via the controller of the connected automated vehicle. Such an implementation allows us to perform experiments on straight roads and at realistic vehicle speeds (up to 24 [m/s]) while keeping the drivers and controllers focused on longitudinal car following. These experiments show that by using long-range feedback, the connected automated vehicle can mitigate traffic waves more effectively than when it only uses information from its immediate predecessor (nearest-neighbor feedback). We also demonstrate that these experimental results can be reproduced by numerical simulations using car-following models with model-matched parameters and delays. We note that compared

Manuscript received June 19, 2019; revised April 21, 2020 and October 3, 2020; accepted November 23, 2020. Date of publication December 29, 2020; date of current version May 3, 2022. This work was supported in part by the Mobility Transformation Center, University of Michigan; and in part by the Toyota InfoTechnology Center, Mountain View, CA, USA. The Associate Editor for this article was Y. Wang. *(Corresponding author: Sergei S. Avedisov.)*

Sergei S. Avedisov is with the Department of Mechanical Engineering, University of Michigan, Ann Arbor, MI 48109 USA (e-mail: sergei.avedisov@toyota.com).

Gaurav Bansal is with Airbus A^3 Labs, Sunnyvale, CA 94086 USA (e-mail: gauravbs@gmail.com).

Gábor Orosz is with the Department of Mechanical Engineering, University of Michigan, Ann Arbor, MI 48109 USA, and also with the Department of Civil and Environmental Engineering, University of Michigan, Ann Arbor, MI 48109 USA (e-mail: orosz@umich.edu).

Digital Object Identifier 10.1109/TITS.2020.3043323

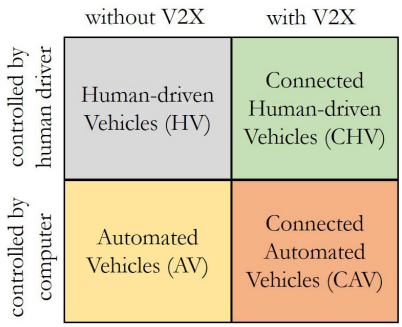

Fig. 1. Vehicle types discussed in this paper.

to our previous work [33], here we consider additional experimental data to highlight the effects of long-range feedback. These experimental results are used to establish a simulation study, the other key focus of this paper.

Since the car-following models are able to replicate the traffic patterns observed in the experiments, we develop simulations of connected vehicle networks to asses the impact of connected automated vehicles on mixed traffic. We investigate networks with different penetrations of connected and connected automated vehicles. These simulations show that when connected automated vehicles use information from multiple vehicles ahead their longitudinal motion control is significantly more effective at improving the throughput of the traffic network than automated vehicles using information solely from their immediate predecessor. This demonstrates that the cognizance connected automated vehicles gain from V2X communication is key to benefiting mobility of future roadways.

The paper is organised as follows. In Section II we discuss the vehicular composition of the connected vehicle network (CVN) and the dynamics of the different types of vehicles in the CVN. In Section III we describe our connected vehicle experiments and the observed traffic patterns. We extend our study to larger connected vehicle networks via numerical simulation in Section IV. In Section V we take a look at traffic patterns of the simulated network with human drivers as well as connected automated vehicles at partial penetration. We then perform a study where we investigate the effect of penetration of connected vehicles on traffic flow in Section VI. Finally, we present our remarks about the experimental and simulation results in Section VII.

II. Connected Vehicle Network

Based on whether a vehicle is controlled by a human operator or a computer and whether it is equipped with V2X communication we distinguish four different types of vehicles as shown in Figure 1. Regular human-driven vehicles (HVs) do not have V2X capabilities. By adding V2X devices they become connected human-driven vehicles (CHV). A vehicle whose dynamics are controlled by a computer is referred to as an automated vehicle (AV) if it only relies on sensory information or a connected automated vehicle (CAV) when it also utilizes V2X connectivity. In this paper we focus on the impact of connectivity on the traffic flow so we assume that all automated vehicles are equipped with V2X devices, i.e., they are all connected automated. However, we construct our controllers so that they still function when no other vehicles in the neighborhood have V2X capability, in which case a connected automated vehicle "degrades" to an automated vehicle. That is, we consider a connected vehicle network composed of regular human-driven vehicles (HVs), connected human-driven vehicles (CHVs), and connected automated vehicles (CAVs) as shown in Figure 2.

As we are looking into mixed traffic containing HVs, CHVs and CAVs, it is important to note our assumptions with regards to how automated vehicles interact with human-driven vehicles and vice versa. On one hand in literature there is a growing realization that the interactions between human driving dynamics in relation to automated vehicles are more subtle, but also more important than often assumed. These human interactions are difficult to capture by mathematical models but they are responsible for some observable phenomena in traffic including intra-driver differences [34], [35]. However, in this paper we assume that human drivers react to CAVs in the same way that they react to other human drivers which we found to be a good approximation of when drivers focus on car following. Moreover, for CAVs we use Connected Cruise Control (CCC) [25], where the CAV does not distinguish whether the sensory or V2V information is coming from a human-driven vehicle or an automated vehicle. We note that we validated this design using multiple experiments with a real connected automated vehicle [25].

In this section we describe longitudinal dynamics of the different types of vehicles using the principles of car-following and decentralized network control.

A. Longitudinal Vehicle Dynamics

We consider a connected vehicle network with N vehicles and denote the position of the rear bumper of vehicle i by s_i and its velocity by v_i; see Figure 2. We neglect tire slip, suspension dynamics, aerodynamic drag, rolling resistance, grade, and engine dynamics. Then the longitudinal motion is described by

$$\begin{aligned} \dot{s}_i(t) &= v_i(t), \\ \dot{v}_i(t) &= f_{\text{sat}}(u_i(t)), \end{aligned} \tag{1}$$

where the dot represents differentiation with respect to time t, u_i gives the scaled driving force commanded by the vehicle operator, and the saturation function f_{sat} represents the limits of the engine and brakes of the vehicle. In particular, we use

$$f_{\text{sat}} = \begin{cases} u_{\min}, & \text{if } u \le u_{\min}, \\ u, & \text{if } u_{\min} < u < u_{\max}, \\ u_{\max}, & \text{if } u \ge u_{\max}, \end{cases} \tag{2}$$

shown in Figure 3A with limits $u_{\max} = 3\,[\text{m/s}^2]$ and $u_{\min} = -10\,[\text{m/s}^2]$, as these correspond to full throttle acceleration and emergency braking observed in experiments [25].

B. Regular Human-Driven Vehicles

For regular human-driven vehicles (HVs) the human driver exhibits two kinds of longitudinal vehicle control: car following and collision prevention. During car following the

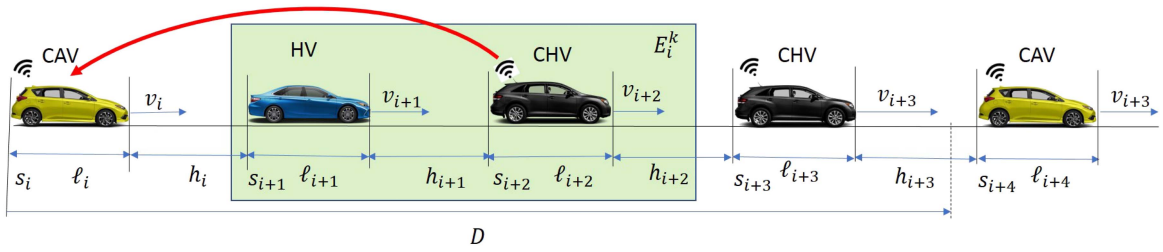

Fig. 2. Connected vehicle network, featuring regular human-driven vehicles (HVs, blue), connected human-driven vehicles (CHVs, black), and connected automated vehicles (CAVs, yellow).

vehicle is tracking the motion of the vehicle directly ahead and chooses the acceleration based on the distance headway (distance to the rear bumper of the preceding vehicle) and the relative velocity. We adopt a model from [36], [37] and assume that the driver of vehicle i responds to the motion of the preceding vehicle using the nonlinear controller

$$u_i^{\mathrm{hf}}(t) = \alpha_i\big(V_i(h_i(t-\tau_i)) - v_i(t-\tau_i)\big) + \beta_i\big(W_i(v_{i+1}(t-\tau_i)) - v_i(t-\tau_i)\big), \quad (3)$$

where τ_i represents the sum of the driver reaction time and the actuation delay while α_i and β_i are control gains for the distance headway and relative velocity feedback, respectively. The superscript hf denotes human car following.

The distance headway feedback term in (3) involves the nonlinear function $V_i(h)$ called the range policy or optimal velocity function [37] which satisfies the following properties:

1) $V_i(h)$ is continuous and monotonically increasing (the more sparse the traffic is, the faster the vehicles want to travel).
2) $V_i(h) \equiv 0$ for $h \le h_{\mathrm{st},i}$ (in dense traffic vehicles intend to stop).
3) $V_i(h) \equiv v_{\max,i}$ for $h \ge h_{\mathrm{go},i}$ (in sparse traffic vehicles intend to travel with the maximum speed).

These properties are satisfied by the function

$$V_i(h) = \begin{cases} 0, & \text{if } h \le h_{\mathrm{st},i}, \\ v_{\max,i}\left(1 - \left(\dfrac{h_{\mathrm{go},i} - h}{h_{\mathrm{go},i} - h_{\mathrm{st},i}}\right)^2\right), & \text{if } h_{\mathrm{st,i}} < h < h_{\mathrm{go,i}}, \\ v_{\max,i}, & \text{if } h \ge h_{\mathrm{go},i}, \end{cases} \quad (4)$$

shown by the blue curves in Figures 3 B and C. Note that the grey points in these figures represent experimental data collected from the experiments described in Section III and the Appendix. The parameters of these range policies are the mean values given in the first two rows of Table I, and these were determined from experiments by model matching as detailed in Section III-B and the Apppendix.

Also W_i is a saturation function for the velocity feedback, that prevents car i from following the predecessor if $v_{i+1} > v_{\max,i}$.

$$W_i(v) = \begin{cases} v, & \text{if } v < v_{\max,i}, \\ v_{\max,i}, & \text{if } v \ge v_{\max,i}, \end{cases} \quad (5)$$

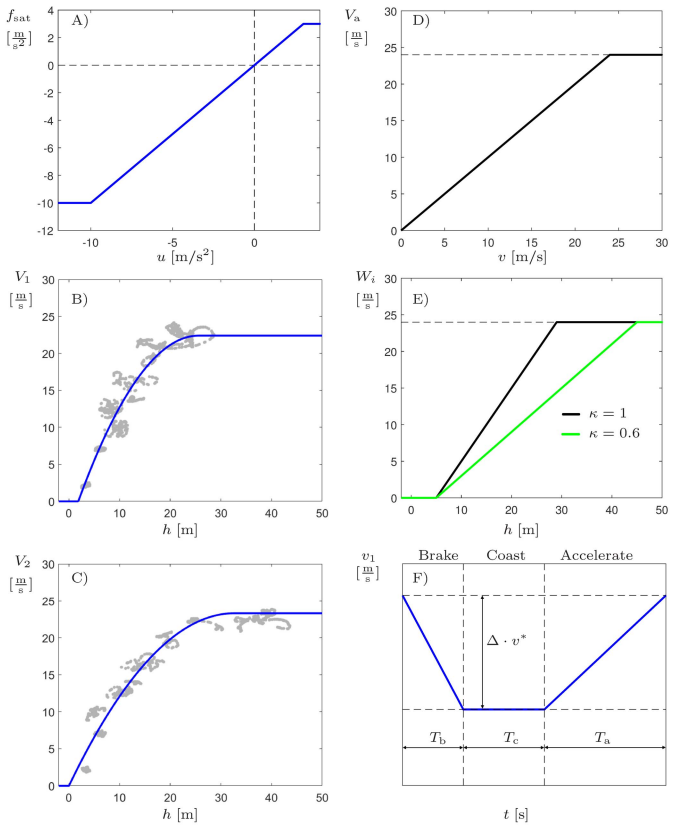

Fig. 3. A) Saturation function for the acceleration of vehicles. B) Experimentally fitted range policy (4) for vehicle 1 with grey points representing experimental data; C) Experimentally fitted range policy (4) for vehicle 2 with grey points representing experimental data D) Speed saturation function (5) E) Designed range policy (11) for the connected automated vehicle F) Perturbation profile for vehicle 1.

see Figure 3 D where $v_{\max} = 24$ [m/s].

In order to define the collision prevention dynamics of human-driven vehicles we define the time to collision of car i as

$$T_i(t) = \frac{h(t) - h_{\mathrm{st},i}}{v_i(t) - v_{i+1}(t)}. \quad (6)$$

We consider that vehicle i is at risk of collision when $T_i(t) < T_c$, i.e.,

$$v_i(t) > v_{i+1}(t) + \frac{1}{T_c}(h(t) - h_{\mathrm{st},i}), \quad (7)$$

where T_c is the critical time-to-collision. When this happens, we assume that the driver of the vehicle i tries to maintain the

TABLE I
RANGE POLICY PARAMETERS FOR VEHICLES IN CONNECTED VEHICLE NETWORK

Vehicle	Parameters		
1	$h_{\mathrm{st},1} = 1.56 \pm 0.12$ [m]	$h_{\mathrm{go},1} = 29.1 \pm 0.92$ [m]	$v_{\max,1} = 24.6 \pm 1.2$ [m/s]
2	$h_{\mathrm{st},2} = -0.20 \pm 0.11$ [m]	$h_{\mathrm{go},2} = 33.9 \pm 0.64$ [m]	$v_{\max,2} = 24.0 \pm 0.6$ [m/s]
3[a]	$h_{\mathrm{st,a}} = 5$ [m]	$h_{\mathrm{go,a}} = 45$ [m] when $\kappa = 0.6$ [1/s] and $h_{\mathrm{go,a}} = 29$ [m] when $\kappa = 1$ [1/s]	$v_{\max,\mathrm{a}} = 24$ [m/s]

[a] Since CAV parameters are designed, no error is given.

critical time-to-collision using the controller

$$u_i^{\mathrm{hc}}(t) = \dot{v}_{i+1}(t-\tau_{\mathrm{c}}) + \frac{1}{T_{\mathrm{c}}}\Big(v_{i+1}(t-\tau_{\mathrm{c}}) - v_i(t-\tau_{\mathrm{c}})\Big), \quad (8)$$

where τ_{c} is the delay associated with the human reaction time in safety-critical situations and the superscript hc refers to this being the human-driven vehicles motion under collision prevention. The commanded longitudinal acceleration of human-driven vehicle i is then

$$u_i(t) = \begin{cases} u_i^{\mathrm{hf}}(t), & \text{if} \quad T(t-\tau_{\mathrm{c}}) \geq T_{\mathrm{c}}, \\ u_i^{\mathrm{hc}}(t), & \text{otherwise.} \end{cases} \quad (9)$$

We note that while implementing the collision prevention mode significantly reduces the chances and severity of collisions, we do not have a proof that the collision prevention mode prevents collisions. In fact this is an active research area with one promising solution being barrier functions [38], [39].

C. Connected Vehicles

Recall from Figure 1 that connected human-driven vehicles (CHVs) are human-driven vehicles equipped with V2X communication devices, enabling them to transmit and receive wireless messages. We also note that connected automated vehicles also have the same capability in terms of communication. We refer to any vehicle that uses V2X communication as a connected vehicle (CV). We note that connected vehicles can interact in different ways including sharing their status, their future intent, and coming to agreements on cooperating maneuvers [40].

In this paper we consider the simplest status sharing class of communication where connected vehicles exchange their position and speed data via the basic safety messages (BSMs) [41]. Messages are broadcast intermittently with a sampling time of Δt. Here we use $\Delta t = 0.1$ [s] corresponding to the dedicated short range communication (DSRC) standard [42]. We assume that each connected vehicle samples its motion data at time instances $t_k = k\,\Delta t$, $k = 0, 1, 2, \ldots$ that can be achieved at a few millisecond accuracy in V2X devices available in the market. When a connected vehicle transmits a packet, another connected vehicle may receive the packet. According to our experiments with the vehicles and devices shown in Figure 4 E, F, there is no significant packet loss if the vehicles are within 300 [m] of each other in a highway environment. Thus, we consider that vehicles can communicate up to 300 [m] distance.

We remark that the way humans can interpret and react to wireless information (if they are provided such) can be complex and relates to human factors [34], [35]. For our study we assume that drivers of connected human-driven vehicles (CHVs) are not given information about the V2X messages received. Consecutively, these vehicles have the same dynamic behavior as the regular human-driven vehicles, i.e., by (3-9).

D. Connected Automated Vehicles

In addition to sending and receiving V2X messages, a connected automated vehicle (CAV) utilizes the obtained information to control its motion. We assume that the CAV uses a combination of sensory information about the vehicle immediately ahead and data received from multiple vehicles ahead via V2V communication to command its longitudinal acceleration. Similar to human-driven vehicles, CAVs may also run in car following or collision prevention modes.

In car-following mode given a processing and actuation delay τ_{a}, the acceleration of the CAV i is commanded by

$$u_i^{\mathrm{af}}(t) = a\Big(V_{\mathrm{a}}\big(h_i(t_k-\tau_{\mathrm{a}})\big) - v_i(t_k-\tau_{\mathrm{a}})\Big) + b\Big(W_{\mathrm{a}}(\bar{v}_i(t_k-\tau_{\mathrm{a}})) - v_i(t_k-\tau_{\mathrm{a}})\Big), \quad (10)$$

which is held constant during the time interval $t \in [t_k, t_{k+1})$ using a zero order hold. The superscript af denotes automated car following, while a and b are control gains for the distance headway feedback term and relative velocity feedback terms according to configuration in Figure 4 D. Also, we design the piecewise linear range policy

$$V_{\mathrm{a}}(h) = \begin{cases} 0, & \text{if} \quad h \leq h_{\mathrm{st,a}}, \\ \kappa(h - h_{\mathrm{st,a}}), & \text{if} \quad h_{\mathrm{st,a}} < h < h_{\mathrm{go,a}}, \\ v_{\max,\mathrm{a}}, & \text{if} \quad h \geq h_{\mathrm{go,a}}, \end{cases} \quad (11)$$

with the parameters provided in the third row of Table I. The corresponding function is plotted in Figure 3 E for different values of κ. Such a design gives an intuitive interpretation to the middle section of the range policy where the slope is given by $\kappa = \frac{v_{\max,\mathrm{a}}}{h_{\mathrm{go,a}} - h_{\mathrm{st,a}}}$, has a unit of [1/s], and can be adjusted to tune the "aggressiveness" of the CAV's controller. In our case, the slope is set to $\kappa = 1$ [1/s] and $\kappa = 0.6$ [1/s] depending on the scenario. The velocity feedback features the weighted average velocity $\bar{v}_i^{(\mathrm{d})}$ of the vehicles located downstream of CAV i, that is,

$$\bar{v}_i(t_k) = \sum_{j \in E_i^k} w_{i,j}(t_k) v_j(t_k), \quad \text{s.t.} \sum_{j \in E_i^k} w_{i,j}(t_k) = 1. \quad (12)$$

The set E_i^k denotes the downstream vehicles including the immediate predecessor of vehicle i ($j = i+1$) whose motion information can either be obtained via V2V (if $i+1$ is connected) or range sensors (if $i+1$ is a regular human-driven vehicle) and the connected vehicles within look-ahead distance D that are traveling slower than vehicle $i+1$; see [43]. In the

specific case shown in Figure 2 we have $E_i^k = \{i+1, i+2\}$. The CAV $i+4$ is beyond the look-ahead distance D, while CHV $i+3$ is traveling faster than the vehicle $i+1$. As the number of vehicles in E_i^k may change in time, the parameters a and b must be carefully tuned to prevent stability loss. We tune the parameters to $a = 0.4$ [1/s] and $b = 0.5$ [1/s] as we found these values to ensure good stability properties as the number of vehicles in E_i^k is varied. We established that $\tau_{\rm a} = 0.5$ [s] in prior experiments with this CAV. Finally, $W_{\rm a}$ is given by (5), as in human-driver car following using $v_{\max,{\rm a}}$.

In collision prevention mode we command the acceleration of the automated vehicle as

$$u_i^{\rm ac}(t) = \dot{v}_{i+1}(t_k - \tau_{\rm a}) + \frac{1}{T_{\rm c}}(v_{i+1}(t_k - \tau_{\rm a}) - v_i(t_k - \tau_{\rm a})), \tag{13}$$

which is held constant during the time interval $t \in [t_k, t_{k+1})$ using a zero order hold. That is, the overall longitudinal acceleration is given by

$$u_i(t) = \begin{cases} u_i^{\rm af}(t), & \text{if} \quad T(t - \tau_{\rm a}) \geq T_{\rm c}, \\ u_i^{\rm ac}(t), & \text{otherwise}, \end{cases} \tag{14}$$

in the time interval $t \in [t_k, t_{k+1})$.

III. Small Scale Experiments

In this section we introduce the experimental setup that allows us to evaluate traffic patterns in a connected vehicle network. We then demonstrate that the traffic patterns observed in the performed experiments can be replicated by simulating the models proposed in the previous section.

A. Setup

Since our goal is to evaluate large-scale traffic patterns in connected vehicle networks such as homogeneous flow or congestion waves, we are interested in how velocity fluctuations propagate along vehicle chains. A common way in the literature to study such problems is to place N vehicles on a circular road of length L [1], [8], [27], [37]. This leads to a periodic boundary condition since the $N+1$-st and the 1-st vehicle become the same. Moreover, the average spacing of the vehicles

$$h_{\rm avg}^* = \frac{1}{N}\Big(L - \sum_{i=1}^{N} \ell_i\Big), \tag{15}$$

can be controlled by adjusting the ring length L and/or the number of vehicles N.

This configuration may allow one to study traffic patterns such as homogeneous flow or traveling waves depending on parameters in the longitudinal dynamics and the average spacing (15). This configuration was used in [28] to demonstrate the formation on traffic jams with human-driven vehicles, while in [30] and automated vehicle was placed among human-driven cars and it was shown that it can mitigate congestion by keeping a large distance to its predecessor. However, the speeds and vehicle spacings achieved in these experiments had to be kept low (below 10 [m/s]) in order to keep the lateral acceleration within a comfortable limit and allow drivers to focus on longitudinal control rather than steering. That is, this setup makes it very challenging to evaluate the traffic patterns for realistic speeds.

To solve this problem we propose to use V2V connectivity in order to establish periodic boundary conditions without having vehicles to drive on a ring. The key idea is to allow that head vehicle of an open chain to observe the motion of the tail vehicle of the chain. Then, by adding the "virtual ring length" L to the longitudinal coordinate of the last vehicle it can be virtually placed ahead of the connected automated vehicle (CAV) as illustrated in Figure 4 A,C for a three-vehicle chain [33]. In this case, the head vehicle (yellow) is a CAV which is followed by two CHVs. Then using $s_1 + L$ in the controllers of the connected automated vehicle the black car can be "placed" in front of it. This setup allows the human drivers to drive at realistic speed ranges (tested up to 24 [m/s]) while maintaining the periodic boundary condition via V2V communication.

Moreover, the established periodic boundary condition allows one to evaluate the impact of an automated vehicle on traffic flow for different values of L (and average vehicle spacings). Indeed, the idea can be extended to scenarios when a connected automated vehicle responds to the motion of multiple vehicles ahead and allows us to evaluate the impact of connected automated vehicles on traffic flow. In the experiments wireless vehicle-to-vehicle (V2V) communication is realized using the devices shown in Figure 4 E. They consist of an electronic control unit and an antennae which transmits basic safety messages (BSM) using standardized Dedicated Short Range Communication (DSRC) protocol [42]. The information broadcasted includes position and velocity. The devices are powered through a 12 Volt power outlet and can be retrofitted to any regular vehicle. The vehicles shown in Figure 4 D are equipped with such V2V devices. Moreover, the vehicle on the right is also capable of automated driving. In particular, the throttle and the brakes can be commanded based on the data received from the other vehicles via V2V communication.

B. Experimental Results

We performed experiments on a straight public road with the connected automated vehicle set up so that the connected vehicles were in the communication range at all times. For the nearest-neighbor feedback we used $E_3^k = \{1\}$ and weight $w_{3,1} = 1$ [1/s] while for the long-range feedback we used $E_3^k = \{1, 2\}$ and weights $w_{3,1} = 0.4$ [1/s], $w_{3,2} = 0.6$ [1/s]. Also, we considered scenarios with $\kappa = 0.6$ [1/s] and $\kappa = 1.0$ [1/s] to observe the effects of the "aggresiveness" of the automated vehicle. In particular, we studied three scenarios as outlined in Table II. Each set of κ and L (and consequently the average vehicle spacing $h_{\rm avg}^*$) was varied, as seen in Table II to account for different homogeneous flow speeds up to about 24 [m/s]. For each experiment the vehicles started from a stationary configuration and then were given some time to approach either a steady state, where they traveled close to homogeneous flow, or to reach steady oscillatory

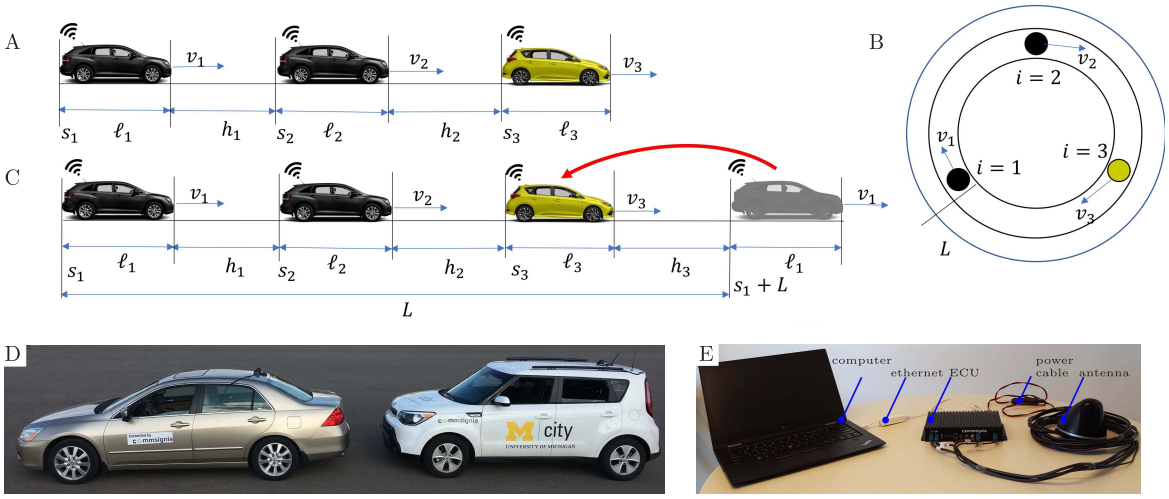

Fig. 4. A) Connected vehicle network with human-driven connected vehicles (black) and a connected automated vehicle (yellow); B) Representation of the connected vehicle network on a ring road; C) The tail vehicle is projected in front of the head vehicle to provide a periodic boundary condition [33]; D) Actual vehicles used in experiments with a human-driven connected vehicle on the left and a connected automated vehicle on the right [25]; E) V2V devices for connected vehicles [25].

TABLE II
EXPERIMENTAL SCENARIOS FOR THREE CAR CONNECTED VEHICLE NETWORK

Feedback	**Ring Lengths** L	**Average Spacings** h^*_{avg}
$\kappa = 0.6$ [1/s] nearest-neighbor	$\{30, 45, \ldots, 135\}$ [m]	$\{5, 10, \ldots, 40\}$ [m]
$\kappa = 1.0$ [1/s] nearest-neighbor	$\{30, 45, \ldots, 90\}$ [m]	$\{5, 10, \ldots, 25\}$ [m]
$\kappa = 1.0$ [1/s] long-range	$\{30, 45, \ldots, 90\}$ [m]	$h^*_{\text{avg}} \in \{5, 10, \ldots, 25\}$ [m]

behavior during which they periodically slowed down and speeded up.

The first column of Figure 5 shows time profiles of the distance headways and velocities of the three vehicles for $h^*_{\text{avg}} = 20$ [m], with the first two rows corresponding to nearest-neighbor feedback with $\kappa = 0.6$ [1/s], the second two rows corresponding to the nearest-neighbor feedback with $\kappa = 1.0$ [1/s], and the last two rows corresponding to the long-range feedback with $\kappa = 1.0$ [1/s]. For $\kappa = 0.6$ [1/s] (see Figure 5 A, C) the vehicles accelerate from a standstill and approach homogeneous flow, where they travel at a constant velocity around 16 [m/s]. This corresponds to the equilibrium speed predicted by the car following models (see black dashed line). When we set $\kappa = 1.0$ [1/s] (see Figure 5 E, G), the vehicles approach a state where their speed and distance headway oscillate. In this case the homogeneous flow is unstable and the homogeneous flow velocity would be close to 19 [m/s] that is close to the average velocities of the vehicles during the steady oscillations. Lastly, when we introduce long-range feedback with $\kappa = 1.0$ [1/s] vehicles approach homogeneous flow (see Figure 5 J, L). Here, the homogeneous flow velocity is also about 19 [m/s] and the vehicles are able to sustain this state and no oscillations develop. To show that the above traffic behavior is captured by the vehicle models presented in Section II, we also plot the corresponding model-matched simulation results in the right column of Figure 5. In particular, model matching was used to select the parameters α_i, β_i and τ_i for the human-driven vehicles $i = 1, 2$; see the Appendix for details. We found that, while these parameters may vary in time and from driver to driver, using approximations $\alpha_1 = \alpha_2$, $\beta_1 = \beta_2$ and $\tau_1 = \tau_2$ we are able to reproduce the behavior of the individual vehicles and that of the connected vehicle network sufficiently well. From the experiments and the model matched simulations we see that for the one-car-look-ahead configuration, choosing between $\kappa = 0.6$ [1/s] and $\kappa = 1.0$ [1/s] is a tradeoff between speed and stability of homogeneous flow. For a given spacing h^*_{avg} decreasing κ decreases the overall velocity of the vehicles, while increasing κ would make the network more susceptible to developing undesirable oscillations. Note, in the $\kappa = 1.0$ [1/s] scenario in Figure 5 F, H the oscillations in distance headway and velocity continue to increase beyond 40 [s] until they reach steady oscillations. The above tradeoff can be resolved by using a long-range feedback, where even with the more aggressively tuned $\kappa = 1.0$ [1/s] the connected vehicle network is able to sustain homogeneous flow at a higher speed. It is demonstrated that by getting information from multiple vehicles ahead, we are able to improve the throughput of the network without making it susceptible to oscillating behavior. This has been verified by multiple experiments using different initial conditions.

IV. LARGE SCALE SIMULATION SETUP

The experiments on the 3-car connected vehicle network performed in Section III demonstrate that changing the way the connected automated vehicle responds to information from vehicles traveling ahead may influence the behavior of the overall connected vehicle network. In particular, we observed

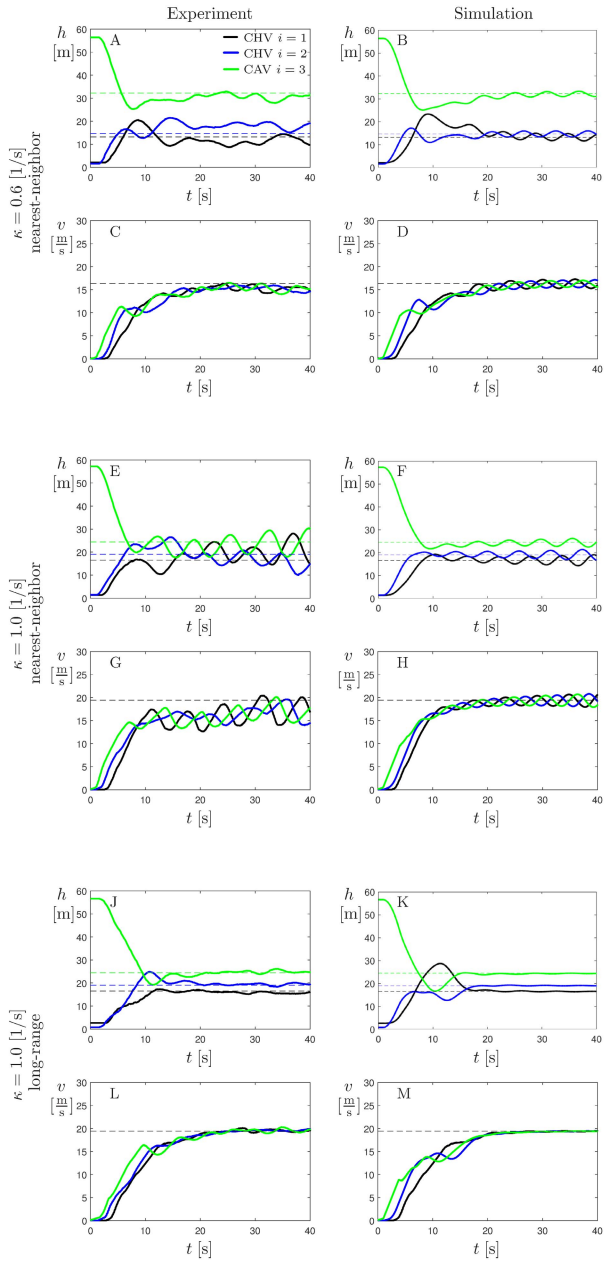

Fig. 5. Time profiles of distance headways and velocities for vehicles in connected vehicle network with average spacing $h^* = 20$ [m] from the experiment (left column) and model matched simulations (right column) for the three scenarios presented in Table II.

that a connected automated vehicle using long-range feedback may allow all vehicles in the network to travel faster and approach homogeneous flow. Furthermore, we demonstrated that for well-tuned parameters the car following models are able to reproduce experimental results.

In this section we investigate effects of connected automated vehicles on traffic by considering connected vehicle networks consisting of regular human-driven vehicles (HVs), connected human-driven vehicles (CHVs), and connected automated vehicles (CAVs). We use the models with parameters determined in the Appendix to characterize human drivers in these simulations. We develop a criterion to baseline the performance of a network of regular human-driven vehicles and then investigate the effects of adding connected vehicles and connected automated vehicles.

A. Connected Vehicle Network Setup

We simulate a connected vehicle network of N vehicles with periodic boundary conditions so that the the first vehicle travels behind the N-th vehicle yielding $s_{N+1} = s_1 + L$ and $v_{N+1} = v_1$ where L is the length of the virtual ring. We emphasize that, similarly to the 3-car network described above, we do not consider ring geometry (that would require to model lateral and yaw dynamics) but rather simply utilize these periodic boundary condition to obtain a closed system. Correspondingly, the distances between the vehicles are calculated using arclengths rather than secants.

Each of the cars is then assigned to be a human-driven vehicle (HV), a connected human-driven vehicle (CHV), or a connected automated vehicle (CAV). We first randomly select $n_{\rm cv}$ vehicles in the network to be connected. Then we select $n_{\rm cav}$ of the connected vehicles to be connected automated. Indeed, the number of connected human-driven vehicles in this network is $n_{\rm cv} - n_{\rm cav}$. We define the connected vehicle penetration rate as $100\frac{n_{\rm cv}}{N}$ % and the connected automated vehicle penetration rate as $100\frac{n_{\rm cav}}{n_{\rm cv}}$ %.

In order to model highway scenarios, we set $h_{\rm st} = 5$ [m] and $v_{\max} = 30$ [m/s] for all drivers, cf. (4) and Figures 3 B,C. To account for the variation between human drivers we assign $h_{\rm go}$ for each human driver from a uniform random distribution in the interval [45, 55] [m]. The other human parameters are set to $\tau_i = 1.0$ [s], $\alpha_i = 0.14$ [1/s] and $\beta_i = 0.54$ [1/s], as determined from model matching; see Appendix. Likewise we adjust the range policy of the CAV so that $v_{\max,a} = 30$ [m/s] while we still use κ to tune the "aggressiveness" of the CAVs; see (11) and Figure 3. We investigate the effects of κ as well as the effects of long-range V2V communication on the global behavior of the constructed connected vehicle networks. Note that even though we set $h_{\rm st} = 5$ [m], vehicles may come to a stop at a headway of less than 5 meters. In our simulations we observed stopping distances of 1 to 5 [m], depending on the driver parameters and the dynamic scenario.

When using long-range feedback the connected automated vehicle i considers connected vehicles up to a look-ahead distance D that are moving slower than the immediate predecessor (vehicle $i+1$). For these vehicles we calculate the weighted downstream velocity $\bar{v}_i^{(\rm d)}$ using (12) with weights

$$w_{ij} = \begin{cases} w_i & \text{if } j = i+1 \\ w_i & \text{if } 0 < s_j - s_i < D \quad \text{and } v_j < v_{i+1}, \\ 0 & \text{otherwise.} \end{cases} \tag{16}$$

Note that we limit the number of vehicles in the set E_i^k to 5, as prior research shows that looking at more than 5 vehicles does not yield significant improvement in performance [25] [44].

One can show that the dynamics of the connected vehicle network (1)-(14) admits a homogeneous flow equilibrium where all the vehicles travel with constant speed while maintaining constant spacings, that is,

$$v_i(t) \equiv v^*, \quad s_{i+1}(t) - s_i(t) - \ell_i \equiv h_i^*, \tag{17}$$

where v^* and h_i^* are the homogeneous flow velocity and homogeneous flow spacing such that

$$v^* = V_i(h_i^*), \quad \sum_{i=1}^{N}(h_i^* + \ell_i) = L. \tag{18}$$

Indeed, we have the average spacing $h_{\text{avg}}^* = \frac{1}{N}\sum_{i=1}^{N} h_i^*$ cf. (15). Depending on the stability of the homogeneous flow, the connected vehicle network may converge to or diverge from the homogeneous flow after a perturbation is introduced. In the latter case traveling waves may form.

B. Testing Procedure

We initialize simulations with all cars traveling at homogeneous flow except the first vehicle, whose motion is perturbed according the speed profile shown in Figure 3 F. The magnitude of the perturbation is characterized by a dimensionless quantity $0 \leq \Delta \leq 1$ called severity. When $\Delta = 0$ no perturbation occurs and the car continues to move with the homogeneous flow. When $\Delta = 1$ the perturbed car first decelerates from v^* to 0 at the deceleration rate $a_{\text{min}} < 0$; cf. Figure 3A. This deceleration happens over a time interval $T_{\text{b}} = -v^*/a_{\text{min}}$. Then the car remains stationary for a time interval T_{c}. Finally, the car accelerates back to v^* at the acceleration rate $a_{\text{max}} > 0$ (cf. Figure 3A) over a time $T_{\text{a}} = v^*/a_{\text{max}}$.

For $0 < \Delta < 1$, the selected car reduces its speed by $\Delta \cdot v^*$ during the interval $0 \leq t < T_{\text{b}}$ using a constant deceleration. During $\{T_{\text{b}} \leq t < T_{\text{b}} + T_{\text{c}}\}$ the car coasts at a constant velocity of $(1-\Delta)v^*$. For our simulations we use $T_{\text{c}} = 5\,[\text{s}]$. Lastly, during $T_{\text{b}} + T_{\text{c}} \leq t < T_{\text{b}} + T_{\text{c}} + T_{\text{a}}$ the car increases its speed back to v^* using constant acceleration. During $0 \leq t \leq T_{\text{b}} + T_{\text{c}} + T_{\text{a}}$ the dynamics of the other vehicles in the network are governed by (1)-(14). For $t \geq T_{\text{b}} + T_{\text{c}} + T_{\text{a}}$ the dynamics of all vehicles are governed by these equations. Such perturbation profiles were found effective at destabilizing connected vehicle networks in theoretical studies [1] and experiments [25], and similar profiles were observed in real rush hour traffic [45]. Other perturbation profiles, specifically where a vehicle increases it's speed is important in high density scenarios ($h^* = 10$ to 20 [m]) such as of queue discharges, which are not considered in this paper.

After introducing the perturbation, we observe the response of the network. As we examine the merits of connected automated vehicles in benefiting traffic flow, we select our performance metric to be an average flow

$$q = \frac{1}{N}\sum_{i=1}^{N} q_i, \tag{19}$$

where the time-averaged flow of car i is given by

$$q_i = \frac{N+1}{t_{\text{f}} - t_{\text{set}}}. \tag{20}$$

Here the time t_{set} denotes the time where the simulation converges to a steady behavior and t_{f} is found by solving

$$s_i(t_{\text{f}}) = L + s_i(t_{\text{set}}). \tag{21}$$

In other words we determine the time it takes each vehicle to go around the ring once after the connected vehicle network gets close to steady motion (i.e., when the emerging traffic pattern does not change anymore with time). When vehicle i returns to the same point after going around the ring, $N+1$ vehicles would have traveled through that point. Given this, we can determine the flow from the perspective of car i in (20). We then average these results over all vehicles in the connected vehicle network using (19).

V. Traffic Patterns in Connected Vehicle Networks

In this section we first examine the performance of vehicle networks consisting of regular human-driven vehicles (HVs) while varying the perturbation severity and the traffic density (i.e., the average vehicle spacing h_{avg}^* via adapting the ring length L, cf. (15)). We then investigate the dynamics when connected vehicles and connected automated vehicles are added to the traffic flow.

A. Human-Driven Network

We first look at the performance of a network solely consisting of regular human-driven vehicles in order to establish a baseline to which we can compare the performance of connected vehicle networks.

Our goal is to highlight the effects of average vehicle spacing and perturbation severity on the large-scale traffic patterns. In Figure 6 the behavior of a vehicle network composed of 100 human driven vehicles is shown. In Figures 6 A, C we observe that for $h_{\text{avg}}^* = 35$ [m] a stop-and-go wave develops independent of the size of perturbations introduced to the network. While some of the vehicles are traveling at free flow speed others are stopped in congestion. When the average vehicle spacing is increased to $h_{\text{avg}}^* = 45$ [m], the humans are able to return to the homogeneous flow after a small perturbation, see Figure 6 B, but large perturbations still lead to stop-and-go motion; see Figure 6 D.

In order to better understand the traffic patterns, we plot the average flow (19) as a function of the perturbation severity in Figure 6 E, F, that are generated using 10 different distributions of human drivers to account for the variation in human behavior. The mean values are plotted as points with the standard deviations captured by the error bars. For $h_{\text{avg}}^* = 35$ [m] the flow for all perturbations remains around 1600 [cars/hr]. This is related to the fact that congestion forms for all perturbations for the spacing $h_{\text{avg}}^* = 35$ [m]. For $h_{\text{avg}}^* = 45$ [m] the flow of the network at low perturbations is around 2200 [cars/hr], which corresponds to highway traffic capacity per lane. However, applying perturbations of severity 0.5 and larger the flow reduces to about 1700 [cars/hr] due to congestion waves.

To obtain a relationship between the flow and vehicle spacing, we plot the flow as a function of average vehicle spacing for $\Delta = 0.01$ and $\Delta = 1.0$ in Figure 6 G. We used such extreme perturbations to highlight the different traffic regimes. For $h_{\text{avg}}^* \leq 40$ [m] both small and large perturbations lead to the same flow. For these spacings congestion

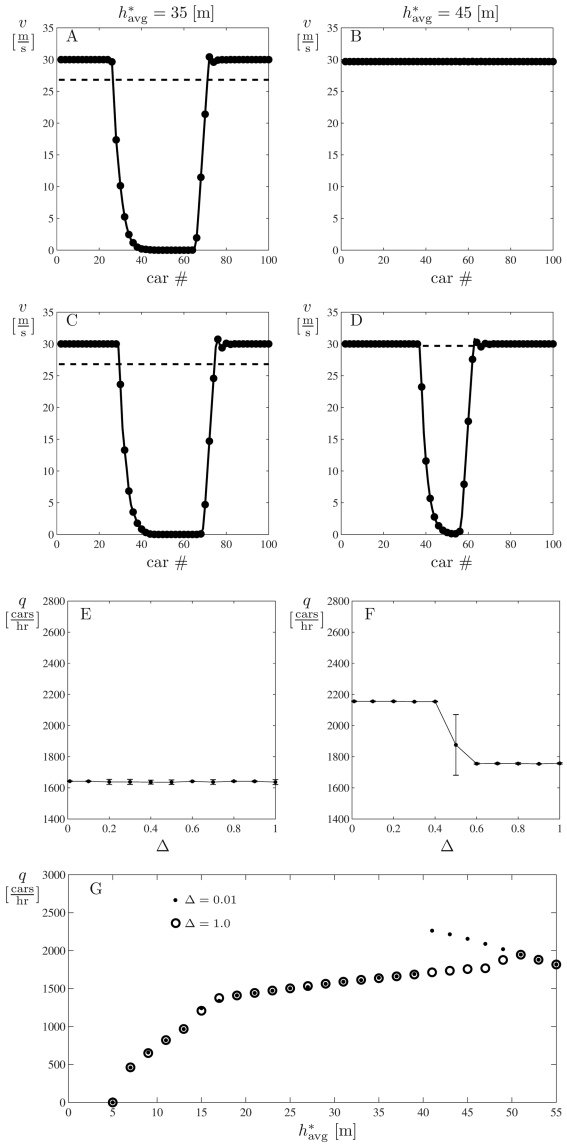

Fig. 6. Behavior of a network consisting of 100 human-driven vehicles. A-D) Distributions of velocities in the network at the end of the simulation for different Δ and h^*_{avg}. The dashed line indicates the homogeneous flow. E, F) Flow-severity charts. G) Flow-spacing chart for different severities as indicated.

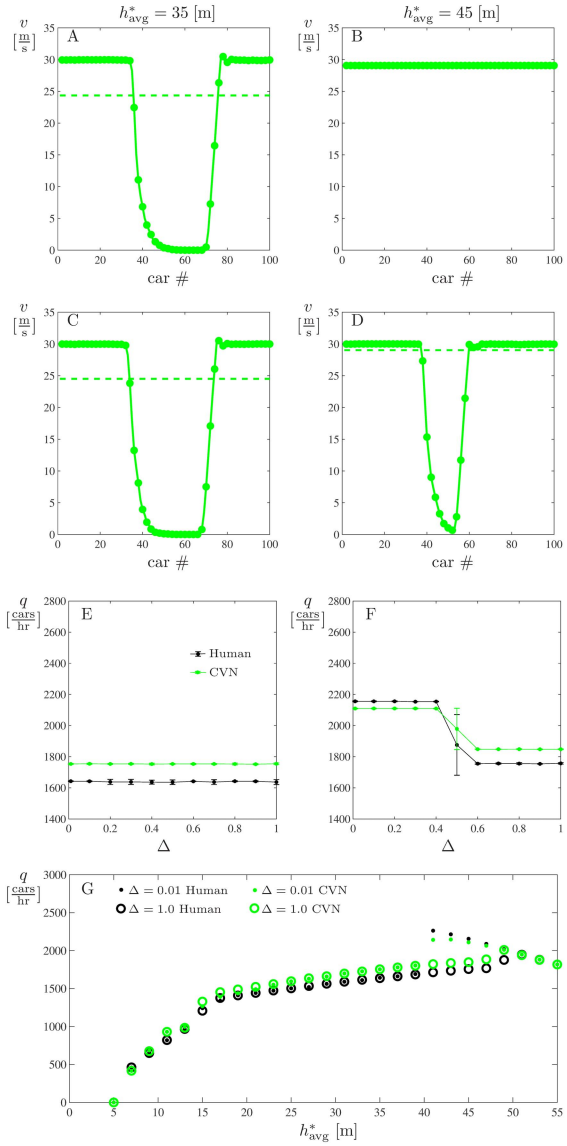

Fig. 7. Behavior of a network with 100% CV penetration and 30% CAV of CV penetration (70% CHVs and 30% CAVs) with the CAVs using nearest neighbor feedback with $\kappa = 0.6$ [1/s] range policy. Same notation is used as in Figure 6.

develops even for a small perturbations, as demonstrated by Figure 6 A, C. For $40 \leq h^*_{avg} \leq 50$ [m] small perturbations result in a significantly higher flow than large perturbations since the human drivers are able mitigate small perturbations while large perturbations trigger congestion, as demonstrated by Figure 6 B, D. For $h^*_{avg} \geq 50$ [m], the flow resulting from small and large perturbations is the same again, since human drivers are able to sustain homogeneous flow for all perturbations examined.

B. Effects of Connected Automated Vehicles

After baselining the performance of the human-driven network, we add connected and connected automated vehicles to the network and examine the performance of the resulting connected vehicle network. As an example, we consider 100% CV penetration and 30% CAV of CV penetration, that is 70 CHVs and 30 CAVs. This represents a scenario in which V2X communication is ubiquitous, but the penetration of automated vehicles is still limited.

First we show that in this scenario of partial penetration of connected automated vehicles, implementing nearest neighbor feedback (where the connected automated vehicle uses information solely from the vehicle immediately ahead) yields marginal benefits to traffic flow as the large-scale traffic patterns do not qualitatively change regardless of whether the connected automated vehicles are tuned to be less or more aggressive ($\kappa = 0.6$ or $\kappa = 1.0$ [1/s]).

Figures 7 and 8 A, C show that for $h^*_{avg} = 35$ [m] stop-and-go waves still develop for large and small perturbations regardless of κ being 0.6 or 1.0 [1/s]. For $h^*_{avg} = 45$ [m], likewise, the connected vehicle network goes to homogeneous flow for small perturbations, and a congestion wave forms for large perturbations for both κ values; cf. Figures 7 B, D

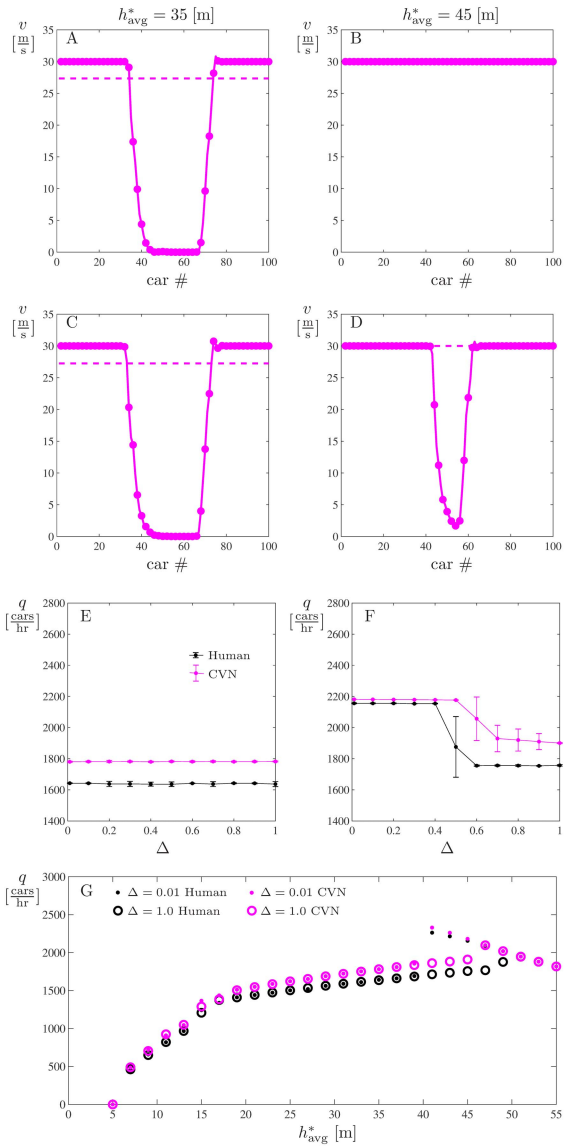

Fig. 8. Behavior of a network with 100% CV penetration and 30% CAV of CV penetration (70% CHVs and 30% CAVs) with the CAVs using nearest neighbor feedback with $\kappa = 1.0$ [1/s] range policy (left). Same notation is used as in Figure 7.

with Figures 8 B, D. However, panel D shows less congestion compared to the human-driven network as vehicles do not stop in congestion.

To account for the distribution of the CAVs in the connected vehicle network, we use the results of 30 different connected vehicle networks with randomly chosen distributions of CAVs in Figures 8 E–G. The points in each of these figures correspond to the mean flow, and the error bars indicate standard deviations. Adding connected automated vehicles leads to a slight (100 [cars/hr]) increase in flow at $h^*_{avg} = 35$ [m] for both the $\kappa = 0.6$ [1/s] and $\kappa = 1.0$ [1/s]; see panel E. For $h^*_{avg} = 45$ [m], using $\kappa = 0.6$ decreases the flow slightly compared to human drivers for perturbations for $\Delta < 0.5$; see Figure 7 F. This can be attributed to larger spacings between vehicles at homogeneous flow in the connected vehicle network. For $\Delta > 0.5$ the connected vehicle network maintains a higher flow than the human-driven network as the congestion for the connected vehicle network is smaller. For $\kappa = 1.0$ [1/s] (Figure 8 F), the connected vehicle network always maintains a slightly higher flow than the human driver network, as the vehicles are closely packed at homogeneous flow and the congestion is less severe for higher perturbations.

Figure 7 G demonstrates that the connected vehicle network with $\kappa = 0.6$ [1/s] performs as good or better than the human-driver network for all h^*_{avg} except between 41 to 45 [m], where for the low perturbations the human-driver network does better. The difference in performance however is not large. When $\kappa = 1.0$ [1/s] (Figure 8 G) the connected vehicle network performs as good or slightly better than the human-driver network without any drawbacks. In particular from $19 \leq h^*_{avg} \leq 39$ the connected vehicle network slightly outperforms the human-driven network for both large and small perturbations. For $41 \leq h^*_{avg} \leq 49$ [m] the connected vehicle network performs better than the human-driver network for large perturbations, and maintains the performance of the human-driver network for small perturbations. Note that in Figures 7 G and 8 G we removed the error bars as the variance between the 30 different configurations as the different distributions of CAVs was not significant.

Now we demonstrate that by using long-range feedback, the connected automated vehicles can significantly improve the flow of the connected vehicle network even at partial penetration. As before, we consider 100% CV penetration and 30% CAV of CV penetration, that is 70 CHVs and 30 CAVs. Figure 9 A shows that at $h^*_{avg} = 35$ [m] the network stays close to homogeneous flow, that is, in steady state the velocities oscillate by 1-2 [m/s]. Congestion does not develop unlike in the human-driven network, or the connected vehicle networks with nearest-neighbor feedback. However, large perturbations still result in stop-and-go congestion; see Figure 9 C. For $h^*_{avg} = 45$ [m], adding the connected automated vehicles with long-range feedback allows for the connected vehicle network to return to homogeneous flow even for large perturbations as demonstrated in Figure 9 D. These changes in traffic patterns are reflected in improvements in flow. In Figure 9 E, we can see that at $h^*_{avg} = 35$ [m] for small perturbations the flow is increased to 2400 [cars/hr], which corresponds to a 50% improvement over the previous networks examined. Moreover, at $h^*_{avg} = 45$ [m] the robustness of the connected vehicle network to perturbations is significantly improved, as the flow stays close to 2200 [cars/hr] for all perturbations.

As depicted in Figure 9 G the most significant improvement in flow over the previous network is for $35 \leq h^*_{avg} \leq 39$ [m] for small perturbations. In the case the connected vehicle network with long-range feedback is able to maintain homogeneous flow for these spacings. The significant flow improvements above give long-range feedback a significant advantage over nearest-neighbor feedback without any significant downsides.

VI. Penetration Study

After seeing that long-range feedback is an effective strategy to improve traffic flow at partial penetrations of connected automated vehicles, we conduct a penetration study to see how many connected and connected automated vehicles are

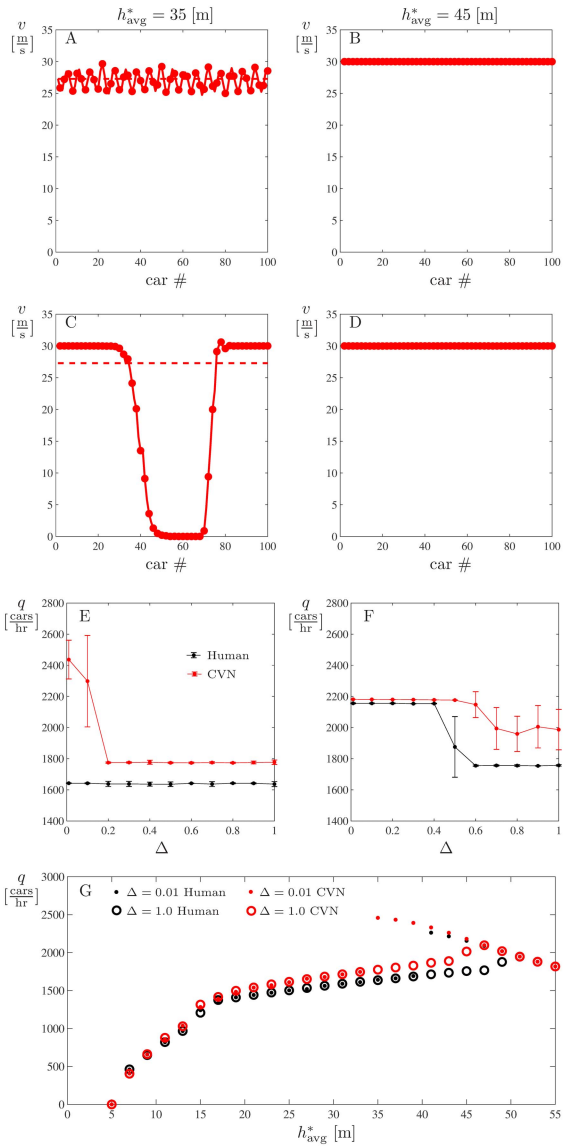

Fig. 9. Behavior of a network with 100% CV penetration and 30% CAV of CV penetration (70% CHVs and 30% CAVs) with the CAVs using long-range feedback with $\kappa = 1.0$ [1/s] range policy. Same notation is used as in Figure 7.

necessary to observe significant benefits in terms of flow. We start with a single distribution of 100 human drivers from the previous section. In this network we vary the CV penetration in increments of 25% from 0% to 100%, which represent how "connected" the traffic environment is. We also vary the CAV of CV penetration in increments of 25% from 0% to 100%, which indicates the fraction of the connected vehicles that are automated. To account for the variability due to different distributions of the CVs and CAVs in the network we use 10 different random distributions of CVs and CAVs to generate results for a given penetration setup.

Because most common perturbations are not severe (it's rare for someone to do a full stop on the highway), we chose to perturb the networks with $\Delta = 0.1$ (corresponding to a 10%) deviation of the speed from homogeneous flow. After the start of the perturbation we let the network run for 5 minutes and calculate the flow as in (19,20,21) with $t_f = 300$ [s]

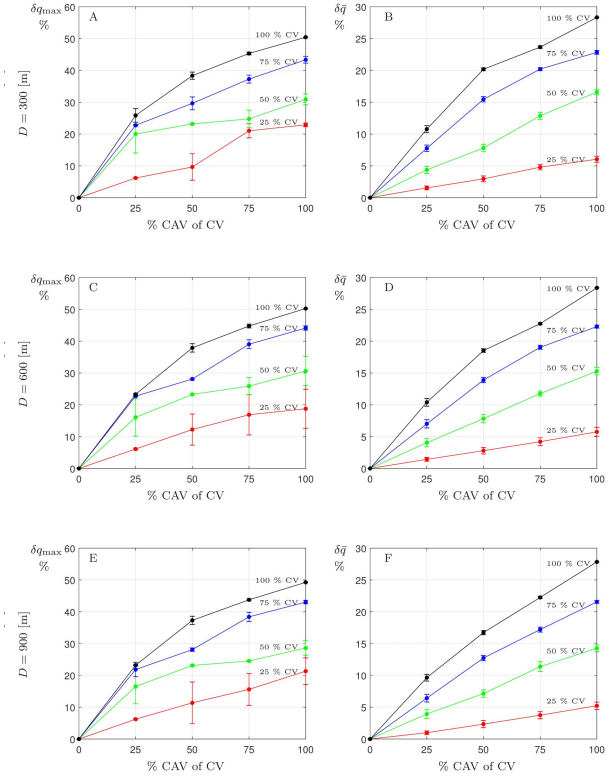

Fig. 10. Penetration study of connected vehicle network with CAV's using long-range feedback A) Maximal flow improvement (22) B) Average flow improvement (23) calculated between $h_{min} = 25$ [m] and $h_{max} = 49$ [m] C, D) Penetration study for $D = 600$, same notation as A,B. E,F) Penetration study for $D = 900$, same notation as A,B.

corresponding to the end of the simulation. The resulting flow of the connected vehicle network as a function of spacing $q_{CVN}(h^*_{avg})$ is compared to that of a network with 100 human-driven vehicles $q_{HVN}(h^*_{avg})$. The first metric we define is the maximum increase in flow over all traffic densities

$$\delta q_{max} = \max_{h \in [h_{min}, h_{max}]} \frac{q_{CVN}(h) - q_{HVN}(h)}{q_{HVN}(h)}. \quad (22)$$

To investigate the change in flow for a wide range of densities, we also consider averaging the flow increase over the densities (between h_{min} and h_{max}) and define another metric

$$\delta \bar{q} = \frac{1}{h_{max} - h_{min}} \int_{h_{min}}^{h_{max}} \frac{q_{CVN}(h) - q_{HVN}(h)}{q_{HVN}(h)} dh. \quad (23)$$

We use $h_{min} = 25$ [m] and $h_{max} = 49$ [m]. The results for both δq_{max} and $\delta \bar{q}$ are shown in Figure 10 A, B, demonstrating that increasing the penetration of CV and CAV increases the performance of CVNs. Also for a given number of CAVs, increasing the number of CHV's yields an improvement in flow. Note in this case we consider vehicles from $D = 300$ [m] ahead as before, as this was the range in which we observed no significant packet losses during experiments.

In Figure 10 A we observe that even when there is 25% CV penetration and 25% CAV of CV penetration (i.e., 25 % connected vehicles and 6 connected automated vehicles in the network), the flow can be increased up to 6 % compared to the human connected vehicle network. With full connectivity (100% CV penetration) just 25% CAV penetration yields 25%

increase in flow. Figure 10 B shows that on average 50% CV penetration and 25% CAV of CV penetration (50 CV's and 13 CAV's) yields close to 5% increase in flow on average over the human-driven network. For full connectivity, even 25 CAV's improve the flow by over 10% on average. Also note that, 50% CV penetration and 25% CAV of CV penetration yields higher metrics than 25% CV penetration and 50% CAV of CV penetration, while both scenarios have 13 connected automated vehicles. Thus, as we mentioned before, for a given number of CAVs increasing the number of CVs leads to an improvement in flow.

In Figures 10 C,D we show the results in which we take D to be 600 [m] rather than 300 [m]. The results are not significantly different for either metric. Even when we increase the look ahead distance to 900 [m], as shown in Figures 10 E,F, there is no significant difference in performance compared to when the CAV's only look ahead 300 [m]. Finally, we remark that when reproducing Figure 10 for different severities of perturbations the qualitative behavior remains the same.

VII. Discussion and Conclusion

To characterize the effect of vehicle-to-vehicle connectivity on traffic patterns, we designed a small-scale experiment featuring three cars: two connected human-driven vehicles and one connected automated vehicle. This experimental setup allowed us to evaluate the effect of different types of feedback used by the connected automated vehicle on traffic patterns at a realistic range of speeds (up to 24 [m/s]). The experiments had important implications. First, using long-range feedback to control the connected automated vehicle gives significant benefits in stability and throughput of the connected vehicle network over nearest-neighbor feedback. Second, car following models perform well in replicating the dynamics of the vehicles as well as the dynamics and traffic patterns arising in the connected vehicle network.

To evaluate the benefits of wireless communication for larger networks we performed simulations of a 100-vehicle connected vehicle network featuring human-driven and connected automated vehicles. We demonstrated that in order for connected automated vehicles to significantly improve traffic flow of the connected vehicle network at low penetration, they must utilize long-range feedback. This is because connected automated vehicles using long range feedback bring changes to traffic patterns that yield significant flow improvements over human-driven traffic, which does not occur when the connected automated vehicles use nearest-neighbor feedback.

Lastly we studied the effects of different penetrations of connected vehicles and connected automated vehicles using long range feedback on traffic flow. We demonstrated that significant benefits for a wide range of traffic densities can be observed with only a few connected automated vehicles, and these benefits increase with the number of connected human-driven vehicles in the network. That is, increasing the penetration of connected human-driven vehicles would enable a small percentage of connected automated vehicles (on the order of 10 to 20 %) to significantly improve the traffic flow. Given that full connectivity can be achieved by a government mandate and off the shelf devices can readily be retrofitted to conventional human-driven vehicles to make them connected [25], [33], these significant improvements can be viable in the near future.

It is also important to discuss the limitations of the assumptions taken in this work. We limited our investigations to traffic patterns that can be generated via single-lane experiments. The analysis performed above can be applied to multi-lane traffic as long as the lane change dynamics do not significantly affect the traffic flow in each lane. When considering lane changes and bottlenecks one may observe additional traffic patterns [26]. We plan to extend our work to such multi-lane highway environments by combining our approaches with well established lane change models such as MOBIL [46].

Another key assumption in this study was limiting the variation of human parameter to the variation in the range policy. In general human driver parameters including the gains, range policies and delays all vary from driver to driver and also for a given driver in time [24], [34], [35]. On the other hand, we expect the parameters of connected automated vehicles to be customizable and vary from CAV to CAV. Statistical studies taking into account these variations may be used to evaluate the robustness of the finding this paper.

The experimental and simulation frameworks developed in this work could allow us to evaluate any other potential control strategies for connected automated vehicles. For instance, with the emergence of reinforcement learning as a technique for control of connected automated vehicles with promising initial simulation results in [31], [47]–[49], it would be interesting to evaluate these algorithms on real vehicles and using large scale simulations to see how they compare in reducing congestion and increasing traffic flow in mixed traffic environments. Finally, our work can be further extended by performing experiments where connected and automated vehicles are mixed into highway traffic which are left for future research.

Appendix
Model-matching human driver behavior

To show that the traffic patterns observed in the experiment can be reproduced by car following models, we select the parameters for the human car-following model (3,4) via a two-step model matching process.

First we fit the range policy (4) to the experimental data to find $h_{\mathrm{st},i}$, $h_{\mathrm{go},i}$, and $v_{\max,i}$. To do this we select segments in the experimental data where the system is close to a homogeneous flow with vehicles traveling at roughly constant speed while maintaining constant distance headways. For example, see the first column with $\kappa = 0.6$ nearest-neighbor feedback and $\kappa = 1$ long-range feedback scenarios in Figure 5. The distance headways and velocities corresponding to these steady states are plotted as grey dots in Figures 3 B, C for vehicles 1 and 2, respectively. The blue curves correspond to the fitted range policies, with parameters given in Table I.

Second we select the appropriate gains α_i, β_i and time delay τ_i for the human drivers in (3). For simplicity, we assume both human drives have similar gains and delays, i.e., $\alpha_i = \alpha_{\mathrm{h}}$, $\beta_i = \beta_{\mathrm{h}}$, $\tau_i = \tau_{\mathrm{h}}$, but our method can be generalized to the scenario

when these parameters are different for each driver. We select the gains and delays by minimizing two cost functions over a range of $\alpha_{\rm h}$, $\beta_{\rm h}$ and $\tau_{\rm h}$.

The first cost function calculates the sum of squared differences between the measured and simulated distance headways and velocities for all cars:

$$J_{\rm car}(\alpha_{\rm h}, \beta_{\rm h}, \tau_{\rm h}) = \frac{1}{t_{\rm end} - t_{\rm st}} \sum_{i=1}^{3} \int_{t_{\rm st}}^{t_{\rm end}} \Big(h_i^{\rm m}(t) - h_i(t)\Big)^2 + C\Big(v_i^{\rm m}(t) - v_i(t)\Big)^2 {\rm d}t. \quad (24)$$

This cost was averaged for all 18 runs (8 for $\kappa = 0.6$ and 5 for $\kappa = 1.0$). The superscript "m" indicates measured quantities, whereas the unsubscripted distance headways and velocities denote data obtained by simulating the network Figure 4 B starting from the same initial condition. Here C is a constant, which we set to 1 [s^2].

The second cost function seeks to match the traffic patterns between the measurements and simulations:

$$J_{\rm trf}(\alpha_{\rm h}, \beta_{\rm h}, \tau_{\rm h}) = \big(\Delta v^{\rm m} - \Delta v\big)^2, \quad (25)$$

where

$$\Delta v = \frac{1}{t_{\rm set}} \int_{t_{\rm set}} \max_{i,j=1,2,3} |v_i(t) - v_j(t)| {\rm d}t, \quad (26)$$

gives the average speed difference between the fastest and the slowest moving vehicle in the connected vehicle network taken over a period of time $t_{\rm set}$ when the network settled down to either homogeneous flow or steady oscillations. More precisely, for the experiments this period of time is taken as a time segment of at least 10 seconds where the trajectories either approach homogeneous flow, or exhibit constant amplitude oscillations. For the simulation results this segment is taken as the last 10 seconds of the simulation. Intuitively small Δv correspond to the network being close to homogeneous flow, whereas large Δv correspond to traffic congestion [1], [27], [37]. This cost was averaged for all 18 runs, and the superscripts are used to distinguish experimental and simulated quantities as in (24).

We select the gains $\alpha_{\rm h}$, $\beta_{\rm h}$ and the delay $\tau_{\rm h}$ for which the values of both of the above cost functions are sufficiently small. For the 18 runs considered we obtained $\alpha_{\rm h} = 0.14$ [1/s], $\beta_{\rm h} = 0.54$ [1/s] and $\tau_{\rm h} = 1.0$ [s]. We show the simulation results with these parameters for $h^*_{\rm avg} = 15$ [m] in the second column of Figure 5. Indeed, the simulations reproduce the experiments with high accuracy in the three scenarios.

ACKNOWLEDGMENT

The authors would like to thank Jin Ge for discussions of the experimental layout, Chaozhe He for assisting with the experiments, and Adam Kiss for discussions on data processing.

REFERENCES

[1] G. Orosz, R. E. Wilson, and G. Stépán, "Traffic jams: Dynamics and control," *Phil. Trans. Roy. Soc. A, Math., Phys. Eng. Sci.*, vol. 368, no. 1928, pp. 4455–4479, Oct. 2010.

[2] D. Helbing, "Traffic and related self-driven many-particle systems," *Rev. Mod. Phys.*, vol. 73, no. 4, pp. 1067–1141, Dec. 2001.

[3] T. Mangel, M. Michl, O. Klemp, and H. Hartenstein, "Real-world measurements of non-line-of-sight reception quality for 5.9GHz IEEE 802.11p at intersections," in *Communication Technologies for Vehicles*. Berlin, Germany: Springer, 2011, pp. 189–202.

[4] M. Sepulcre, J. Gozalvez, B. Coll-Perales, M. Carmen Lucas-Estañ, and J. Ramon Gisbert, "Empirical performance models for V2 V communications," in *Proc. IEEE Int. Conf. Comput. Inf. Technol.; Ubiquitous Comput. Commun.; Dependable, Autonomic Secure Comput.; Pervas. Intell. Comput.*, Oct. 2015, pp. 737–742.

[5] F. Arena and G. Pau, "An overview of vehicular communications," *Future Internet*, vol. 11, no. 2, p. 27, Jan. 2019.

[6] S. van de Hoef, K. H. Johansson, and D. V. Dimarogonas, "Fuel-efficient en route formation of truck platoons," *IEEE Trans. Intell. Transp. Syst.*, vol. 19, no. 1, pp. 102–112, Jan. 2018.

[7] A. Talebpour and H. S. Mahmassani, "Influence of connected and autonomous vehicles on traffic flow stability and throughput," *Transp. Res. C, Emerg. Technol.*, vol. 71, pp. 143–163, Oct. 2016.

[8] S. S. Avedisov and G. Orosz, "Analysis of connected vehicle networks using network-based perturbation techniques," *Nonlinear Dyn.*, vol. 89, no. 3, pp. 1651–1672, 2017.

[9] Y. Zheng, S. E. Li, K. Li, and L.-Y. Wang, "Stability margin improvement of vehicular platoon considering undirected topology and asymmetric control," *IEEE Trans. Control Syst. Technol.*, vol. 24, no. 4, pp. 1253–1265, Jul. 2016.

[10] F. Chou, S. E. Shladover, and G. Bansal, "Coordinated merge control based on V2V communication," in *Proc. IEEE Veh. Netw. Conf. (VNC)*, Dec. 2016, pp. 1–8.

[11] A. I. Morales Medina, N. van de Wouw, and H. Nijmeijer, "Cooperative intersection control based on virtual platooning," *IEEE Trans. Intell. Transp. Syst.*, vol. 19, no. 6, pp. 1727–1740, Jun. 2018.

[12] S. Tsugawa, S. Jeschke, and S. E. Shladover, "A review of truck platooning projects for energy savings," *IEEE Trans. Intell. Vehicles*, vol. 1, no. 1, pp. 68–77, Mar. 2016.

[13] X. Sun and Y. Yin, "Behaviorally stable vehicle platooning for energy savings," *Transp. Res. C, Emerg. Technol.*, vol. 99, pp. 37–52, Feb. 2019.

[14] S. E. Shladover, D. Su, and X.-Y. Lu, "Impacts of cooperative adaptive cruise control on freeway traffic flow," *Transp. Res. Rec., J. Transp. Res. Board*, vol. 2324, no. 1, pp. 63–70, Jan. 2012.

[15] M. Wang, W. Daamen, S. P. Hoogendoorn, and B. van Arem, "Rolling horison control framework for driver assistance systems. part ii: Cooperative sensing and cooperative control," *Transp. Res. C, Emerg. Technol.*, vol. 40, pp. 290–311, 2014.

[16] S. Oncu, J. Ploeg, N. van de Wouw, and H. Nijmeijer, "Cooperative adaptive cruise control: Network-aware analysis of string stability," *IEEE Trans. Intell. Transp. Syst.*, vol. 15, no. 4, pp. 1527–1537, Aug. 2014.

[17] S. E. Shladover, C. Nowakowski, X. Y. Lu, and R. Ferlis, "Cooperative adaptive cruise control: Definition and operating concepts," in *Proc. 94th TRB Annu. Conf.*, 2015, vol. 2489, no. 1, pp. 145–152.

[18] J. Ploeg, N. van de Wouw, and H. Nijmeijer, "Fault tolerance of cooperative vehicle platoons subject to communication delay," in *Proc. 12th IFAC Workshop Time-Delay Syst.*, 2015, pp. 352–357.

[19] V. Milanés and S. E. Shladover, "Handling cut-in vehicles in strings of cooperative adaptive cruise control vehicles," *J. Intell. Transp. Syst.*, vol. 20, no. 2, pp. 178–191, Mar. 2016.

[20] L. Xiao, M. Wang, W. Schakel, and B. van Arem, "Unravelling effects of cooperative adaptive cruise control deactivation on traffic flow characteristics at merging bottlenecks," *Transp. Res. C, Emerg. Technol.*, vol. 96, pp. 380–397, Nov. 2018.

[21] G. Orosz, "Connected cruise control: Modelling, delay effects, and nonlinear behaviour," *Vehicle Syst. Dyn.*, vol. 54, no. 8, pp. 1147–1176, Aug. 2016.

[22] L. Zhang and G. Orosz, "Motif-based design for forward-looking delayed networks with applications to connected vehicle systems," *IEEE Trans. Intell. Transp. Syst.*, vol. 17, no. 6, pp. 1638–1651, Jan. 2016.

[23] W. B. Qin, M. M. Gomez, and G. Orosz, "Stability and frequency response under stochastic communication delays with applications to connected cruise control design," *IEEE Trans. Intell. Transp. Syst.*, vol. 18, no. 2, pp. 388–403, Feb. 2017.

[24] J. I. Ge and G. Orosz, "Connected cruise control among human-driven vehicles: Experiment-based parameter estimation and optimal control design," *Transp. Res. C, Emerg. Technol.*, vol. 95, pp. 445–459, Oct. 2018.

[25] J. I. Ge, S. S. Avedisov, C. R. He, W. B. Qin, M. Sadeghpour, and G. Orosz, "Experimental validation of connected automated vehicle design among human-driven vehicles," *Transp. Res. C, Emerg. Technol.*, vol. 91, pp. 335–352, Jun. 2018.
[26] M. Treiber, A. Hennecke, and D. Helbing, "Congested traffic states in empirical observations and microscopic simulations," *Phys. Rev. E, Stat. Phys. Plasmas Fluids Relat. Interdiscip. Top.*, vol. 62, no. 2, pp. 1805–1824, Aug. 2000.
[27] I. Gasser, G. Sirito, and B. Werner, "Bifurcation analysis of a class of 'car following' traffic models," *Phys. D: Nonlinear Phenomena*, vol. 197, nos. 3–4, pp. 222–241, 2004.
[28] Y. Sugiyama *et al.*, "Traffic jams without bottlenecks—Experimental evidence for the physical mechanism of the formation of a jam," *New J. Phys.*, vol. 10, p. 33001, Mar. 2008.
[29] J. I. Ge, S. S. Avedisov, and G. Orosz, "Stability of connected vehicle platoons with delayed acceleration feedback," in *Proc. ASME Dyn. Syst. Control Conf.*, 2013, Art. no. V002T30A006.
[30] R. E. Stern *et al.*, "Dissipation of stop-and-go waves via control of autonomous vehicles: Field experiments," *Transp. Res. C, Emerg. Technol.*, vol. 89, pp. 205–221, Apr. 2018.
[31] A. R. Kreidieh, C. Wu, and A. M. Bayen, "Dissipating stop-and-go waves in closed and open networks via deep reinforcement learning," in *Proc. 21st Int. Conf. Intell. Transp. Syst. (ITSC)*, Nov. 2018, pp. 1475–1480.
[32] A. K. Kiss, S. S. Avedisov, D. Bachrathy, and G. Orosz, "On the global dynamics of connected vehicle systems," *Nonlinear Dyn.*, vol. 96, no. 3, pp. 1865–1877, May 2019.
[33] S. S. Avedisov, G. Bansal, A. K. Kiss, and G. Orosz, "Experimental verification platform for connected vehicle networks," in *Proc. 21st Int. Conf. Intell. Transp. Syst. (ITSC)*, Nov. 2018, pp. 818–823.
[34] J. van Lint and S. Calvert, "A generic multi-level framework for microscopic traffic simulation—Theory and an example case in modelling driver distraction," *Transp. Res. B, Methodol.*, vol. 117, pp. 63–86, Nov. 2018.
[35] M. Saifuzzaman, Z. Zheng, M. M. Haque, and S. Washington, "Understanding the mechanism of traffic hysteresis and traffic oscillations through the change in task difficulty level," *Transp. Res. B, Methodol.*, vol. 105, pp. 523–538, Nov. 2017.
[36] M. Bando, K. Hasebe, K. Nakanishi, and A. Nakayama, "Analysis of optimal velocity model with explicit delay," *Phys. Rev. E, Stat. Phys. Plasmas Fluids Relat. Interdiscip. Top.*, vol. 58, no. 5, pp. 5429–5435, Nov. 1998.
[37] S. S. Avedisov and G. Orosz, "Nonlinear network modes in cyclic systems with applications to connected vehicles," *J. Nonlinear Sci.*, vol. 25, no. 4, pp. 1015–1049, Aug. 2015.
[38] A. D. Ames, J. W. Grizzle, and P. Tabuada, "Control barrier function based quadratic programs with application to adaptive cruise control," in *Proc. 53rd IEEE Conf. Decis. Control*, Dec. 2014, pp. 6271–6278.
[39] C. R. He and G. Orosz, "Safety guaranteed connected cruise control," in *Proc. 21st Int. Conf. Intell. Transp. Syst. (ITSC)*, Nov. 2018, pp. 549–554.
[40] SAE, "Taxonomy and definitions for terms related to cooperative driving automation for on-road motor vehicles," SAE International J3216_202005, 2020.
[41] SAE, "On-Board System Requirements for V2V Safety Communications," SAE International, SAE J2945/1_201603, 2016.
[42] SAE, "Dedicated short range communications (DSRC) message set dictionary set," SAE International, SAE J2735SET_201603, 2016.
[43] S. S. Avedisov and G. Bansal, "Vehicle mitigation system," U.S. Patent 15 403 064, Jul. 19, 2018.
[44] J. I. Ge and G. Orosz, "Optimal control of connected vehicle systems with communication delay and driver reaction time," *IEEE Trans. Intell. Transp. Syst.*, vol. 18, no. 8, pp. 2056–2070, Aug. 2017.
[45] T. G. Molnár, D. Upadhyay, M. Hopka, M. Van Nieuwstadt, and G. Orosz, "Exploiting V2X connectivity by delayed Lagrangian continuum traffic models," *Transp. Res. C*, to be published.
[46] A. Kesting, M. Treiber, and D. Helbing, "General lane-changing model MOBIL for car-following models," *Transp. Res. Rec., J. Transp. Res. Board*, vol. 1999, no. 1, pp. 86–94, Jan. 2007.
[47] C. Wu *et al.*, "Framework for control and deep reinforcement learning in traffic," in *Proc. IEEE 20th Int. Conf. Intell. Transp. Syst. (ITSC)*, Oct. 2017.
[48] E. Vinitsky, K. Parvate, A. Kreidieh, C. Wu, and A. Bayen, "Lagrangian control through deep-RL: Applications to bottleneck decongestion," in *Proc. 21st Int. Conf. Intell. Transp. Syst. (ITSC)*, Nov. 2018, pp. 759–765.
[49] R. Cheng, G. Orosz, R. M. Murray, and J. W. Burdick, "End-to-end safe reinforcement learning through barrier functions for safety-critical continuous control tasks," in *Proc. 33rd AAAI Conf. Artif. Intell.*, 2019, pp. 3387–3395.

Sergei S. Avedisov (Member, IEEE) received the M.Sc. and Ph.D. degrees in mechanical engineering from the University of Michigan, Ann Arbor, USA, in 2016 and 2019, respectively. He currently works with Toyota Research and Development InfoTech Labs, as a Connected Automated Driving Engineer. His research interest includes longitudinal and lateral control of connected automated vehicles.

Gaurav Bansal received the bachelor's degree in electrical engineering from the Indian Institute of Technology, Kanpur, and The University of British Columbia. He is a Principal Engineer with Airbus A^3 Labs where he is currently leading initiatives in Artificial Intelligence to enable self-piloted aircraft operation and flying autonomous vehicles. Previously, he worked as a Principal Researcher with the Toyota InfoTechnology Center, Mountain View, CA, USA, where he lead several research efforts on the design of communication systems for automated driving. He is an Expert in vehicular communications, pioneering contributions in Dedicated Short Range Communications (DSRC) congestion control and in innovative use-cases to leverage connectivity in vehicles. He represented Toyota in the Automakers Vehicle Safety Communication Consortium and in the SAE and ETSI standardization bodies. His research interest includes millimeter wave and full-duplex wireless communications. His paper on DSRC Congestion Control received the Best Paper Award from the IEEE WiVEC Symposium. He also holds several patents in the field. He serves on the Editorial Board for IEEE *Vehicular Technology Magazine* and IEEE CONNECTED VEHICLES INITIATIVE.

Gábor Orosz (Member, IEEE) received the M.Sc. degree in engineering physics from the Budapest University of Technology, Hungary, in 2002, and the Ph.D. degree in engineering mathematics from the University of Bristol, U.K., in 2006. He held the post-doctoral positions with the University of Exeter, U.K., and the University of California, Santa Barbara, before joining the University of Michigan, Ann Arbor, in 2010. He is currently an Associate Professor of Mechanical Engineering and Civil and Environmental Engineering. His current research interests include nonlinear dynamics and control, time-delay systems, machine learning with applications on connected and automated vehicles, and biological networks.